 

# Radicals in the Mechanochemical Dechlorination of Hazardous Organochlorine Compounds Using CaO Nanoparticles

**Tadaaki Ikoma,* Qiwu Zhang, Fumio Saito, Kimio Akiyama, Shozo Tero-Kubota, and Tatsuhisa Kato†**

Institute of Multidisciplinary Research for Advanced Materials, Tohoku University, Sendai 980-8577

†Institute for Molecular Science, Okazaki National Research Institutes, Okazaki 444-8585

(Received April 18, 2001)

For the first time, we detected paramagnetic products generated during the grinding of 3-chlorobiphenyl (BP-Cl) with calcium oxide (CaO) nanoparticles by a ball mill method, which is one of the promising ways to detoxify hazardous chlorinated organic compounds. Those products were assigned to oxygen-centered aromatic radicals coming from BP-Cl and trapped electrons in oxygen vacancies on the surfaces of the CaO reactants using high-frequency and pulsed electron paramagnetic resonance spectroscopies. The observed good correlation between the dechlorination efficiency and the radical yield suggests that a radical mechanism plays an important role in the destruction of organochlorine compounds. The mechanochemical dechlorination could be interpreted by the following mechanism. First of all, the mechanical stressing induces the electron transfer from $O^{2-}$ sites on the surface of the CaO particle to the organic compounds. The produced organic anion radicals then undergo the effective self-dissociation of a chlorine–carbon bond.

It is widely recognized that hazardous chlorinated organic compounds, such as polychlorodibenzo-*p*-dioxin (dioxin), polychlorobenzofuran and coplanar polychlorobiphenyl (PCB), are pollutants that are the most dangerous to our environment and our health. Such great concern has led to many investigations of the complete decomposition of these toxic compounds. In particular, the waste management of a large volume of PCB, which had been industrially produced and used worldwide as an insulating oil in transformers and as lubricants for high temperature applications, has caused many social problems.[1] Recently, a mechanochemical method with alkaline earth metals (Mg, Ca), or their oxides, has attracted attention as a practically simple and useful process for degrading chlorinated organic compounds,[2,3] while several techniques, such as combustion at a very high temperature, plasma treatment,[4] supercritical water oxidation[5] and so on,[6] have been developed to dispose of PCB and products contaminated with PCB. Therefore, for the sake of improving the mechanochemical process, it is desired to investigate the reaction mechanism of dechlorination on the reactant surface.

Electron paramagnetic resonance (EPR) spectroscopy is one of the useful experimental techniques available for understanding the surface structures[7,8] and reactions in the solid state.[9–13] Especially, because the high-frequency EPR[14,15] and pulsed EPR[16,17] methods can achieve substantial resolution enhancement of the spectrum, we have been able to investigate heterogeneous and disordered systems in detail. In this work, these EPR spectroscopies were used to study the reaction mechanism in the mechanochemical dechlorination of organochlorine using inorganic nanoparticles as a reactant. In order to focus attention on the reaction mechanism, 3-chlorobiphenyl (BP-Cl) was adopted as the simplest model molecule for PCB, because only BP-Cl among the three monochlorobiphenyl isomers is liquid at room temperature, like PCB. It was found that the grinding of BP-Cl with a suitable reactant generated a large amount of trapped electrons and oxygen-centered organic radicals. We discuss a possible radical mechanism, including an electron transfer at the primary step in the mechanochemistry.

## Experimental

Commercial reagents of BP-Cl (Lancaster) and $Ca(OH)_2$ (Wako Pure Chemical) were used without further purification. CaO was prepared by heating $Ca(OH)_2$ at 800 °C for 2 hours. A planetary ball mill (Fritsch Pulverisette-7) was used to grind mixtures of BP-Cl/CaO and BP-Cl/$Ca(OH)_2$ at approximately 700 rpm within a zirconia pot. An o-ring sealed the reaction pot in order to avoid the influence of atmospheric oxygen molecules and moisture.[18,19] BP-Cl and the reactants were mixed in a weight ratio of 3:7. The mixtures were charged into a reaction pot of 45 $cm^3$ inner volume with seven zirconia balls of 15 mm diameter. The morphology of the inorganic reactants was observed with a scanning electron microscope (SEM, Hitachi S-900).

EPR measurements were carried out with three types of EPR apparatus: X-band (9.6 GHz, Bruker ESP-380E and ELEXES E580), Q-band (34 GHz, Bruker ESP-300E) and W-band (94 GHz, Bruker ELEXES E680) spectrometers. A standard dielectric resonator with a low $Q$ factor was used for hyperfine sublevel correlation spectroscopy (HYSCORE). A helium gas-flow system (Oxford ESR-900) was utilized to control the measurement temperature in the range of 4–300 K. 2,2-Diphenyl-1-picrylhydrazyl (DPPH) free radicals (Tokyo Kasei) recrystallized from an ethanol solvent were used as a standard for measuring the spin concentration. HYSCORE at the X-band frequency was performed using four microwave pulses, as illustrated in Fig. 1. The widths of the

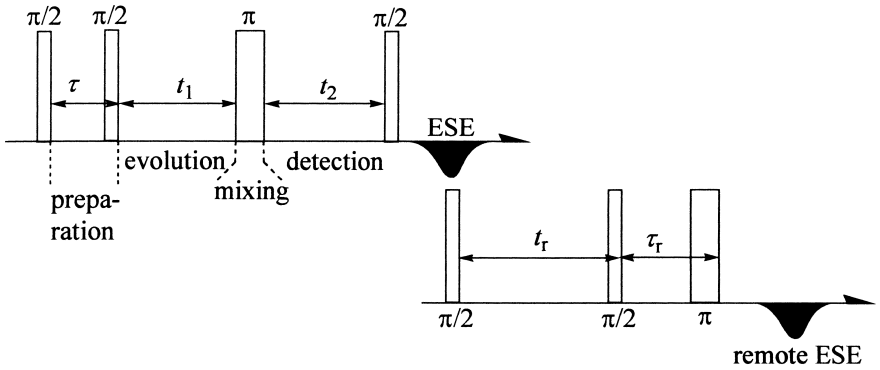


Fig. 1. Microwave pulse sequence for the four-pulse HYSCORE experiment. The last three pulses in the low line form the sequence for a remote echo method employed when $\tau$ was shorter than the dead time of the spectrometer (88 ns). The time delays of $t_r$ and $\tau_r$ for the remote detection were fixed at 400 ns and 128 ns, respectively.

$\pi/2$ and $\pi$ pulses were 8 ns and 16 ns, respectively. The two-dimensional time domain signal was acquired by recording the amplitude of the stimulated electron spin echo (ESE) as a function of $t_1$ and $t_2$, which correspond to the evolution and the detection periods, respectively. The nuclear modulation effect on the time domain signal $S(t_1, t_2)$ was extracted by subtracting the non-modulating components from the original data. It was then converted into the two-dimensional frequency domain spectrum of $S(\nu_1, \nu_2)$ by a double Fourier transformation. Because the preparation period of $\tau$ influences the spectral intensity, a so-called blind spot effect,[20] we measured the HYSCORE spectra at several $\tau$ values. As shown in Fig. 1, we employed a remote echo detection method,[21] when it was necessary to measure at $\tau$ times shorter than the dead time of the spectrometer used (88 ns).

## Results

The mean size of the CaO and $Ca(OH)_2$ particles before milling was about 10 μm. However, as shown in Fig. 2, the mill treatment produced fine primary particles in several tens of nm size, and considerably increased the specific surface area of the reactants. As previously reported for PCB,[2] the BP-Cl substance was also destroyed by grinding together with the CaO nanoparticles. On the other hand, such effective destruction of BP-Cl did not take place by employing $Ca(OH)_2$ instead of CaO, although the conditions for the mixing ratio and the grinding time were the same as in the case of BP-Cl/CaO.

As shown in Fig. 3, strong EPR signals were detected for the ground BP-Cl/CaO mixture at room temperature, although the BP-Cl/$Ca(OH)_2$ mixture did not give any reliable EPR signals. The observed X-band EPR spectrum of the BP-Cl/CaO mixture is likely to be comprised of sharp and broad signals. Both signals increased in intensity with the grinding time, as shown in Fig. 4. The spin concentrations of the sharp and broad signals, which were estimated by a comparison with the EPR intensity of the DPPH radical diluted in KBr powder, were roughly equal during the growth. It was confirmed by gas chromatography–mass spectroscopy that the depletion of

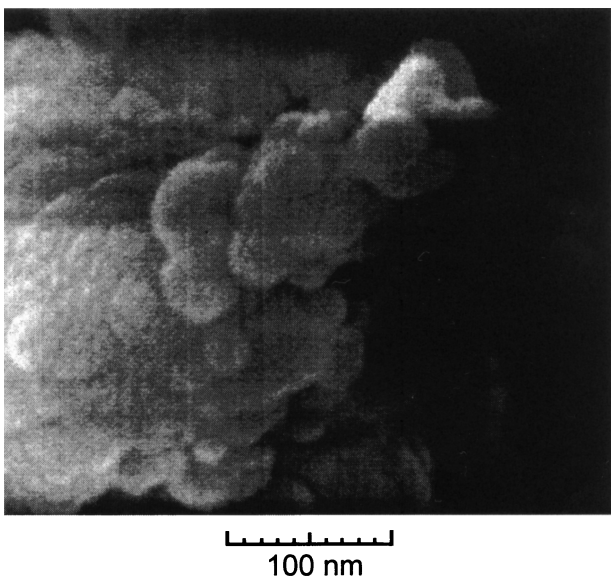


Fig. 2. SEM image of the CaO reactant ground in a ball mill for 360 min.

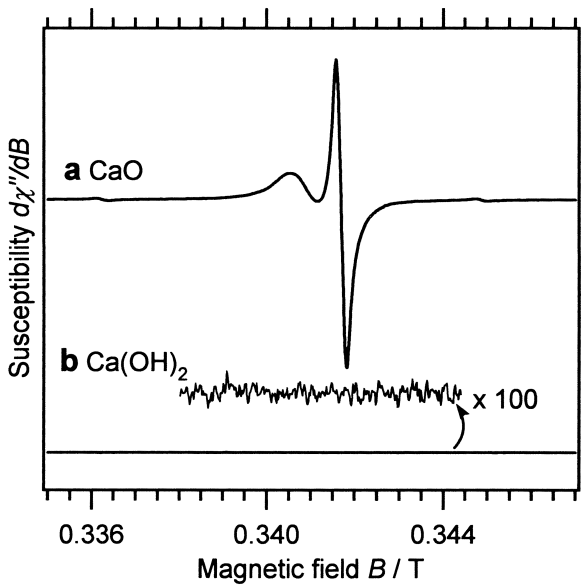


Fig. 3. X-band EPR spectra of the BP-Cl/CaO mixture (a) and the BP-Cl/$Ca(OH)_2$ mixture (b) ground in a ball mill. The spectra were obtained by a 100 kHz field modulation of 0.2 mT at room temperature.

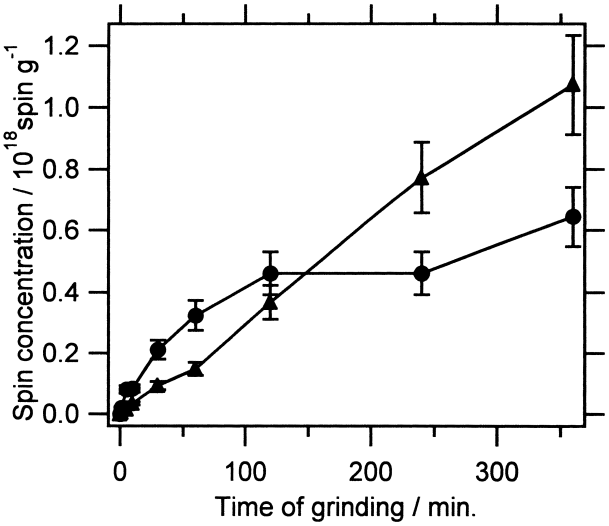


Fig. 4. Grinding time dependence of the yield for the paramagnetic products generated by milling the BP-Cl/CaO mixture. ● and ▲ express the concentrations for the oxygen-centered aromatic radicals and the trapped electrons evaluated from the broad and the sharp EPR signals, respectively.

BP-Cl also progressed with the grinding time. More than 99% BP-Cl was destroyed after milling for 360 min. The monotonic increase in the EPR signals indicates that the paramagnetic products were generated through the destruction of BP-Cl. The disappearance of EPR signal in the case of grinding with $Ca(OH)_2$ particles suggests that the paramagnetic products can be characteristic for effective destruction. In other words, radical reactions may occur in the dechlorination process of BP-Cl by the mechanochemical method.

The low spectral resolution of the EPR signals around 0.341 T at the X-band frequency, which corresponds to the $g$ value for free electron spin ($g_e$), makes an unambiguous assignment of the paramagnetic species difficult. Therefore, we measured the high-frequency EPR spectra for the ground BP-Cl/CaO sample. Figure 5 shows the EPR spectra of the BP-Cl/CaO mixture measured using three types of microwaves with different frequencies. The spectra displayed in this figure are an integrated lineshape of the first-derivative signals obtained by a conventional phase-sensitive-detection system. We can see that the signals are well resolved due to the difference in the $g$ values as the microwave frequency increases. Very sharp lines appeared at $g = 2.0000$ and 1.9994. It was also clarified that broad signals were present from $g = 2.0028$ to $g = 2.0050$. These sharp lines are safely assigned to the trapped electrons on the surface of CaO, namely an S center of which the $g$ factor is smaller than $g_e$ and the $g$ anisotropy is relatively narrow.[22] On the other hand, the $g$ values for the broad signals are comparable to the principal $g$ values for organic radicals containing oxygen atoms, such as phenoxy and quinonoid radicals.[23,24] The lineshape of the broad EPR spectrum can be interpreted in terms of uniaxial $g$ anisotropy caused by the oxygen atoms.

For the sake of characterizing the oxygen-centered organic radicals, we measured the HYSCORE spectra of the broad signals, which enhance the frequency resolution by the nuclear

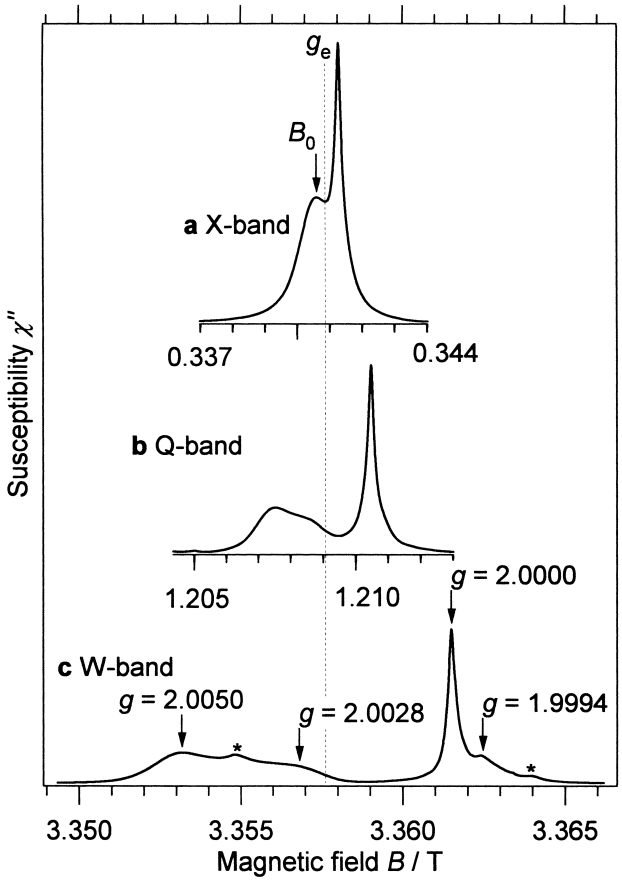


Fig. 5. EPR spectra of the BP-Cl/CaO mixture ground for 360 min measured at X-band of 9.553 GHz (a), Q-band of 33.884 GHz (b) and W-band of 94.096 GHz (c) microwave frequencies. These absorption lineshapes were obtained from numerical integration of the differential signals observed at room temperature by virtue of a conventional field modulation technique at 100 kHz. The external magnetic field was calibrated by adopting a standard $Mn^{2+}$ sample in MgO. $g_e$ is 2.0023 corresponding to the value for a free electron, and $B_0$ in (a) indicates the magnetic field for the HYSCORE measurements. The humps marked with an asterisk arise from an $Mn^{2+}$ impurity in the CaO crystals.

modulation effect.[25] Figure 6 shows the HYSCORE spectrum of $\tau = 136$ ns observed at the top of the broad EPR signal. The $\tau$ time is an optimized preparation period for the hyperfine signals of $^{13}C$. Well-resolved correlation signals were detected in the area from 0 MHz to 20 MHz. The axes of both $\nu_1$ and $\nu_2$ in Fig. 6 depict the electron spin echo envelope modulation (ESEEM) frequency that corresponds to the energy separations among the nuclear spin levels interacting with the unpaired electron. The nuclear Zeeman splittings of $^{43}Ca$, $^{35}Cl$, $^{13}C$ and $^{1}H$ are, respectively, 1.0, 1.4, 3.7 and 14.5 MHz under the used external magnetic field. According to the Larmor frequencies of these nuclei ($\nu_n$), the weak signal at ($\nu_C$, $\nu_C$) on the diagonal is assigned to the $^{13}C$ atoms interacting weakly with the unpaired electron. The signal in the lower frequency region stems from $^{43}Ca$ or $^{35}Cl$, but distinguishing them is difficult to do within the present experimental accuracy because of the

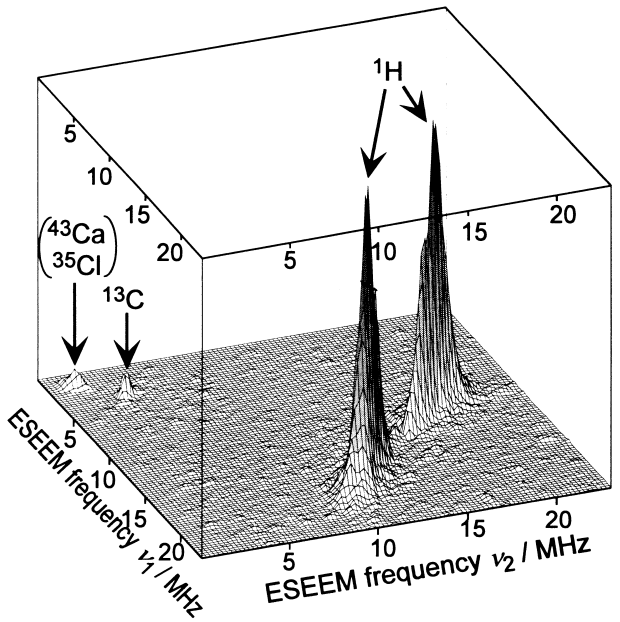


Fig. 6. Stack plot of the HYSCORE spectrum for the aromatic radicals produced by grinding the BP-Cl/CaO mixture. The spectrum was measured at $\tau$ = 136 ns at room temperature.

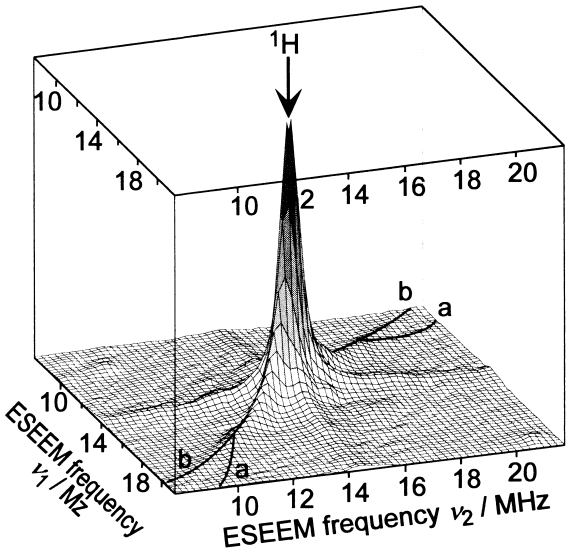


Fig. 7. Stack plot of the $^1$H-HYSCORE spectrum for the aromatic radicals generated by grinding the BP-Cl/CaO mixture. The spectrum was measured at $\tau$ = 36 ns at room temperature. The solid lines of a and b indicate the signal ridges bent by the anisotropic hyperfine interactions of $^1$H.

small difference between $\nu_{Ca}$ and $\nu_{Cl}$. The two strong signals in off-diagonal, which connect around the diagonal points of ($\nu_H$, $\nu_H$), have been identified as the hyperfine spectra due to $^1$H nuclei. Because the blind spot effect of $\tau$ = 136 ns strongly suppresses the signals near ($\nu_H$, $\nu_H$), we cannot see any signals around the $^1$H-Larmor frequency. The ridges of the $^1$H-hyperfine signals do not extend straight along the $\nu_2 = -\nu_1 + 2\nu_H$ line. Some components in the outer parts of the $^1$H-spectrum show arched shapes. As a consequence, the apparent ridge width increases upon going out of the diagonal position of ($\nu_H$, $\nu_H$). In the HYSCORE spectrum for a disordered sample, the anisotropy of the hyperfine interaction leads not only to a broadening of the correlation signal, but also to a bending of the ridge of the signal.[26] A similar HYSCORE spectrum was observed at very low temperatures. No obvious hyperfine signals due to $^{35}$Cl appeared in the HYSCORE spectra measured, even at very low temperatures at the optimized time ($\tau$) for $^{35}$Cl (344 ns). No hyperfine splitting signal of $^{35}$Cl indicates that the organic radical products did not possess chlorine. On the other hand, it is considered that the low natural abundance of $^{13}$C (1.11%) results in the observation of no clear $^{13}$C-hyperfine signals.[27]

In order to avoid any blind-spot effect on the $^1$H-hyperfine signals, we measured the HYSCORE spectrum at $\tau$ = 36 ns, which is an adequate time for $^1$H. A strong signal reduced by the blind spot effect of $\tau$ = 136 ns appeared around the $^1$H-Zeeman position of ($\nu_H$, $\nu_H$), as shown in Fig. 7. This fact indicates that many protons having small hyperfine splittings are present within the radical molecules. A mathematical apodization of the time domain data in the Fourier-transformation procedure induces the cross type of broadening for the intense signal at the $^1$H-Zeeman position, which spreads out along the $\nu_1 = \nu_H$ and $\nu_2 = \nu_H$ lines. The ridge extending along the $\nu_2 = -\nu_1 + 2\nu_H$ line is the hyperfine spectrum due to $^1$H. Two series of arched signals, noted by a and b, are recognized in the outer parts of the $^1$H-hyperfine signals, as indicated by the solid lines.

The location and shape of the correlation peaks of $I = 1/2$ in the HYSCORE spectrum of a disordered sample are easy to understand based on mapping on the $\nu_1^2$ and $\nu_2^2$ coordinates, because of the square root dependence of the ESEEM frequency,[28,29]

$$\nu_2 = \sqrt{Q\nu_1^2 + G}. \quad (1)$$

$Q$ and $G$ include the tensor elements of the hyperfine interaction, depending on the direction of the external magnetic field. In Fig. 8, the observed two bending ridges of $^1$H are illustrated in the $\nu_2^2$ versus $\nu_1^2$ plot. The signal arches of both a and b become straight-line segments. The linearity of the peak position indicates that those signals are broadened by the hyperfine interaction with the same kinds of protons. Each of the lines obtained by fitting the HYSCORE data on a least-square method meets at the two points with the $\nu_2 = -\nu_1 + 2\nu_H$ line. The crossing points are associated with the principal values of hyperfine interaction. The fitting lines go through the common cross section of A. Because of this fact, the series of signals seem to be transformed into the triangular shape of ABC in the $\nu_2^2$ vs $\nu_1^2$ plot, although all of the hyperfine signals are not detected due to the finite band width of the microwave pulses used and the elimination principle of the nuclear modulation effect near the canonical angles. The triangular form suggests the orthorhombic hyperfine interactions of $^1$H. From the distances among the vertexes of A, B and C in the triangle, the isotropic and anisotropic terms of $^1$H-hyperfine interaction were estimated to be $\mp$5.7 MHz and ($\pm$0.1, $\pm$ 4.2, $\mp$4.3) MHz, respectively. The obtained anisotropy for the $^1$H-hyperfine interaction is consistent with that of the $\alpha$-protons of $\pi$-

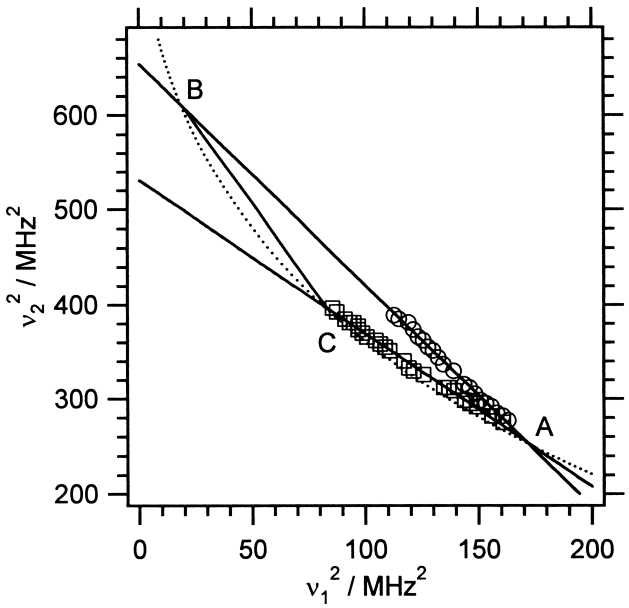


Fig. 8. $\nu_1^2 - \nu_2^2$ plot of the two ridges of $^1$H-hyperfine signals in the HYSCORE of the aromatic radicals generated by grinding the BP-Cl/CaO mixture. ○ and □ respectively depict the series-a and -b in Fig. 7. The locations for the two ridges were extracted from the HYSCORE spectra measured at several $\tau$ times. The straight lines of AB and AC were independently obtained by fitting each series of experimental data. The broken line is defined by $\nu_2 = -\nu_1 + 2\nu_H$.

radicals.[30] The $\pi$ spin density on the carbon ($\rho$) giving the triangle HYSCORE ridges was determined to be 0.011 ± 0.002, according to the proportionality of the hyperfine interaction to $\rho$. On the other hand, intense signals around the $^1$H-Zeeman position indicate the existence of many carbons holding spin densities of less than 0.01. These spin densities are comparable to the values for some of the carbons in the oxygen-centered $\pi$-radicals having a few aromatic rings, in which the oxygen has the largest amount of spin density and the carbons also retain more or less the spin densities conducted through the $\pi$-conjugated network.[24]

## Discussion

The high-frequency EPR and the two-dimensional ESEEM spectroscopies have clarified that the paramagnetic products of the trapped electrons ($e^-$) on the CaO particles and the oxygen-centered aromatic radicals (Ar-O$^\bullet$) are generated during the mechanochemical destruction of BP-Cl with CaO. Based on the experimental facts of the effective dechlorination of BP-Cl and the detection of these radical products, a surface reaction on the CaO particles can be proposed as shown in Scheme 1.

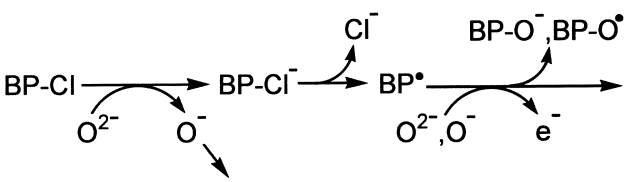


Scheme 1.

In general, alkaline earth metal oxides, such as MgO, CaO and SrO, form a face-centered cubic crystal structure, like rock salts. Their activated surfaces, which are usually achieved by irradiation or a heat treatment under vacuum, function as a strong reducing site for adsorbed molecules.[31–34] The persistent cleavage of the CaO crystal induced by grinding in a closed ball mill continues to supply new surfaces that have never been exposed to the air. Although BP-Cl can encounter both of the $Ca^{2+}$ and $O^{2-}$ ion sites on the surfaces, the reaction at $O^{2-}$, rather than $Ca^{2+}$, may be effective because of the large radii of the negative ion. The contact of BP-Cl with a clean oxygen-rich surface would result in an electron transfer from the $O^{2-}$ ion to the organic substance, and would yield a BP-Cl anion radical (BP-Cl$^-$) and an oxygen atom ion ($O^-$). The halogen in aromatic anion radicals has a tendency to dissociate as an anion because of the strong electronegativity and the relatively weak bond between the carbon and the halogen.[35] Hence, BP-Cl$^-$ is also expected to undergo self-dissociative dechlorination on the CaO crystal surface, generating a reactive biphenyl radical (BP$^\bullet$) and a stable ionic chlorine ($Cl^-$).[36,37] The mechanochemically-induced electron transfer as the primary reaction is probably a key step in effectively inducing the dechlorination in this system. Various radical reactions may be initiated from BP$^\bullet$. A reaction of BP$^\bullet$ with reactive oxygens, such as $O^{2-}$ and $O^-$, is one of the radical reactions leading to biphenyl anions with oxygen (BP-O$^-$) oxygen-centered radicals (BP-O$^\bullet$). During this addition reaction of oxygen, electrons may be released from the reactive oxygens and be captured in a deep vacancy surrounded by five neighboring $Ca^{2+}$ ions, where the oxygen atoms were originally located. BP-O$^-$ and BP-O$^\bullet$ may undergo further reactions, for instance ring additions, rearrangements and so on. Several kinds of oxygen-centered aromatic radicals (Ar-O$^\bullet$) can be generated from these reactions. As a whole, solid state reactions, the relatively stable paramagnetic species of Ar-O$^\bullet$ and $e^-$, are accumulated during the destruction of BP-Cl by the radical mechanism.

The observed spin concentration after 360 min grinding corresponds to ca. 1 mol% yield of radical converted from BP-Cl. We confirmed that the EPR signal disappeared for a solution prepared by washing the ground sample with an ethyl acetate solvent. Based on this fact, the high-concentrated radical in solid phase seems to be related to the immobility and stabilization of radical molecules on the CaO particles, although the aromatic radicals can be reactive in the solution phase. On the other hand, no detection of the paramagnetic $O^-$ species by EPR is understood based on fast hydrogen abstractions from organic molecules due to the high reactivity of $O^-$.

The low-yield destruction of BP-Cl during grinding with $Ca(OH)_2$ is interpreted in terms of inefficient primary electron transfer between the substance and the reactant. $O^{2-}$ tends to function as a Lewis base stronger than $OH^-$ on the surface of various catalysts. Thus, a primary electron transfer from $OH^-$ to BP-Cl hardly takes place. As a result, the radical yield becomes negligible. This chemical insight was theoretically verified. An ab initio molecular–orbital theory calculation using a 6–31G basis function set[38] showed that the energy level of the highest occupied orbital for the $O^{2-}$ ion, which is the outermost atomic 2*p* orbital, is drastically stabilized due to protonation. Taking into account the energy difference in the outer va-

lence electrons, the nature of electron donation for $O^{2-}$ would be stronger than that for $OH^-$.

Grinding has been reported to induce dislocations in the crystal structure of alkaline earth oxides and to generate surface-trapped electrons.[39] The trapped electron can act as an electron-donating center for adsorbates with a small reduction potential ($|E_{red}|$).[32] We also confirmed the surface-trapped electrons derived from milling only CaO powder using the EPR method. The yield of the trapped electrons was two-orders lower than that of a BP-Cl/CaO mixture. Therefore, the trapped electrons in the point vacancy defects that are created by the CaO crystal cleavage, itself, do not contribute much to the primary electron transfer reaction, because of the relatively low encounter frequency with the substance.

## Conclusion

We found that the radical products were generated from grinding BP-Cl with the CaO nanoparticles by which the hazardous organochlorine could be effectively dechlorinated. The radical products increased in concentration with the grinding time of the BP-Cl/CaO mixture. On the other hand, when we used $Ca(OH)_2$ instead of CaO as the reactant, BP-Cl scarcely yielded the dechlorinated compounds and the radical products. The multifrequency and two-dimensional EPR spectroscopies allowed us to assign the radical species in disordered heterogeneous samples. The detected paramagnetic products were attributed to trapped electrons on the surface of the CaO particles and the oxygen-centered aromatic radicals originating from BP-Cl. A radical mechanism initiated by electron transfer was proposed for the mechanochemistry between the organohalide and the alkaline earth oxides.

Measurements of EPR at low temperatures and SEM were respectively performed with the aid of Mr. M. Sakai (IMS) and Mr. A. Masuhara (Tohoku University). The present study was financially supported by a Grant-in-Aid of Scientific Research (No. 12740310) from the Japan Ministry of Education, Science, Sports and Culture. Thanks are due to the Research Center for Molecular Materials, IMS, for permission to do the high frequency EPR measurements.

## References

1 J. S. Waid, "PCBs and the Environment," CRC Press, Boca Raton (1986).

2 S. A. Rowlands, A. K. Hall, P. G. McCormick, R. Street, R. J. Hart, G. F. Ebell, and P. Donecker, *Nature*, **367**, 223 (1994).

3 G. Cao, S. Doppiu, M. Monagheddu, R. Orrù, M. Sannia, and G. Cocco, *Ind. Eng. Chem. Res.*, **38**, 3218 (1999).

4 J. R. Hollis, *Environ. Progr.*, **1**, 7 (1983).

5 K. Hatakeda, Y. Ikushima, O. Sato, T. Aizawa, and N. Saito, *Chem. Eng. Sci.*, **54**, 3079 (1999).

6 J. P. Woodyard, *Environ. Prog.*, **9**, 131 (1990).

7 B. Xu, X. Chen, and L. Kevan, *J. Chem. Soc., Faraday Trans.*, **87**, 3157 (1991).

8 J.-S. Yu, J. W. Ryoo, and L. Kevan, *J. Chem. Soc., Faraday Trans.*, **93**, 1225 (1997).

9 J. Y. Kim, J.-S. Yu, and L. Kevan, *Mol. Phys.*, **95**, 989 (1998).

10 M. Anpo, S. G. Zhang, and Z. Gu, *Res. Chem. Intermed.*, **21**, 631 (1995).

11 M. Anpo, S. G. Zhang, S. Higashimoto, M. Matsuoka, H. Yamashita, Y. Ichihashi, Y. Matsumura, and Y. Souma, *J. Phys. Chem. B*, **103**, 9295 (1999).

12 T. Watanabe, T. Isobe, and M. Senna, *J. Solid State Chem.*, **122**, 291 (1996).

13 N. Miyajima, T. Akatsu, T. Ikoma, O. Ito, B. Rand, Y. Tanabe, and E. Yasuda, *Carbon*, **38**, 1831 (2000).

14 S. S. Eaton and R. G. Eaton, *Magn. Reson. Rev.*, **16**, 157 (1993).

15 T. F. Prisner, in "Advances in Magnetic and Optical Resonance Vol. 20," ed. by W. S. Warren, Academic Press, San Diego (1997) pp. 245.

16 A. Schweiger, *Angew. Chem., Int. Ed. Engl.*, **30**, 265 (1991).

17 S. A. Dikanov and Y. D. Tsvetkov, "Electron Spin Echo Envelope Modulation (ESEEM) Spectroscopy," CRC Press, Boca Raton (1992).

18 G. Mi, Y. Murakami, D. Shindo, and F. Saito, *Powder Technol.*, **105**, 162 (1999).

19 Q. Zhang and F. Saito, *J. Alloys Comp.*, **279**, 99 (2000).

20 P. Höfer, *J. Magn. Reson. A.*, **111**, 77 (1994).

21 H. Cho, S. Pfenninger, C. Gemperle, A. Schweiger, and R. R. Ernst, *Chem. Phys. Lett.*, **160**, 391 (1989).

22 R. L. Nelson, A. J. Tench, and B. J. Harmsworth, *Trans. Faraday Soc.*, **63**, 1427 (1967).

23 K. Mukai and N. Inagaki, *Bull. Chem. Soc. Jpn.*, **53**, 2695 (1980).

24 J. A. Pedersen, "Handbook of EPR spectra from Quinones and Quinols," CRC Press, Boca Raton (1985).

25 T. Ikoma, O. Ito, S. Tero-Kubota, and K. Akiyama, *Energy & Fuels*, **12**, 996 (1998).

26 E. J. Reijerse and S. A. Dikanov, *Pure & Appl. Chem.*, **64**, 789 (1992).

27 T. Ikoma, O. Ito, S. Tero-Kubota, and K. Akiyama, *Energy & Fuels*, **12**, 1363 (1998). On the basis of the HYSCORE measurements of the aromatic radicals with various molecular sizes, it has been elucidated that the aromatic $\pi$ radicals having more than three benzene rings are able to display the obvious $^{13}C$-hyperfine signals in the first quadrant of spectrum.

28 S. A. Dikanov and M. K. Bowman, *J. Magn. Reson. A*, **116**, 125 (1995).

29 S. A. Dikanov and M. K. Bowman, *J. Bio. Inorg. Chem.*, **3**, 18 (1998).

30 H. M. McConnel, C. Heller, T. Cole, and R. W. Fessenden, *J. Am. Chem. Soc.*, **82**, 766 (1960).

31 M. Chiesa, E. Giamello, D. M. Murphy, G. Pacchioni, M. C. Paganini, R. Soave, and Z. Sojka, *J. Phys. Chem. B*, **105**, 497 (2001).

32 A. M. Volodin, V. A. Bolshov, and T. A. Konovalova in "Radicals on Surfaces," ed. by A. Lund and C. Rhodes, Kluwer Academic Publisher, Dordrecht (1994), pp. 201.

33 A. Zecchina and F. S. Stone, *J. Catalysis*, **101**, 227-237 (1986).

34 K. J. Klabunde, R. A. Kaba, and R. Morris, *Inorg. Chem.*, **17**, 2684 (1978).

35 J. Fossey, D. Lefort, J. Sorba, and G. Ourisson, "Free Radicals in Organic Chemistry," Wiley, New York (1995), Chap. 9.

36 M. Ohashi, K. Tsujimoto, and K. Seki, *J. Chem. Soc., Chem. Commun.*, **1973**, 384.

37 N. J. Bunce, Y. Kumar, L. Ravanal, and S. Safe, *J. Chem. Soc., Perkin Trans. 2*, **1978**, 880.

38 Gaussian 98, Revision A.7, M. J. Frisch, G. W. Trucks, H. B. Schlegel, G. E. Scuseria, M. A. Robb, J. R. Cheeseman, V. G. Zakrzewski, J. A. Montgomery, Jr., R. E. Stratmann, J. C. Burant, S. Dapprich, J. M. Millam, A. D. Daniels, K. N. Kudin, M. C. Strain, O. Farkas, J. Tomasi, V. Barone, M. Cossi, R. Cammi, B. Mennucci, C. Pomelli, C. Adamo, S. Clifford, J. Ochterski, G. A. Petersson, P. Y. Ayala, Q. Cui, K. Morokuma, D. K. Malick, A. D. Rabuck, K. Raghavachari, J. B. Foresman, J. Cioslowski, J. V. Ortiz, A. G. Baboul, B. B. Stefanov, G. Liu, A. Liashenko, P. Piskorz, I. Komaromi, R. Gomperts, R. L. Martin, D. J. Fox, T. Keith, M. A. Al-Laham, C. Y. Peng, A. Nanayakkara, C. Gonzalez, M. Challacombe, P. M. W. Gill, B. Johnson, W. Chen, M. W. Wong, J. L. Andres, C. Gonzalez, M. Head-Gordon, E. S. Replogle, and J. A. Pople, Gaussian, Inc., Pittsburgh PA, 1998.

39 P. Auzins, J. W. Orton, and J. E. Wertz, in "Paramagnetic Resonance," ed. by W. Low, Academic Press, New York (1963), pp. 90.